

The bremsstrahlung-like production of the massive spin-2 dark matter mediator

I. V. Voronchikhin^{1,*} and D. V. Kirpichnikov^{2,†}

¹*Tomsk Polytechnic University, 634050 Tomsk, Russia*

²*Institute for Nuclear Research, 117312 Moscow, Russia*

The link between Standard Model (SM) particles and dark matter (DM) can be introduced via spin-2 massive mediator, G , that couples to photon and charged leptons. Moreover, in a mediator mass range from sub-MeV to sub-GeV, fixed-target facilities such as NA64e, LDMX, NA64 μ , M³, and E137, can potentially probe such particle of the hidden sector via the signatures that are described by the bremsstrahlung-like process involving tensor mediator. We compare numerically the Weizsaker-Williams (WW) approximation and the exact tree-level (ETL) approach for the bremsstrahlung-like mediator production cross section by choosing various parameters of the fixed-target experiments. In addition, we derive novel constraints on spin-2 DM mediator parameter space from the data of the E137 fixed-target experiment. In particular, we demonstrate that the E137 experiment has been ruled out the the couplings of the spin-2 mediator at the level of $8 \times 10^{-8} \text{ GeV}^{-1} \lesssim c_{ee}^G \lesssim 10^{-5} \text{ GeV}^{-1}$ for the typical masses in the range $100 \text{ MeV} \lesssim m_G \lesssim 800 \text{ MeV}$, that corresponds to the statistics of 1.87×10^{20} electrons accumulated on target. The latter implies its universal coupling to photons and leptons, $c_{ee}^G = c_{\gamma\gamma}^G$.

I. INTRODUCTION

During the past few decades, a considerable number of astrophysical observations have led to the concept of the dark sector, where the DM can manifest itself via gravitational effects [1, 2]. In particular, the main indirect evidence of the DM is the galaxy rotation velocities, the cosmic microwave background anisotropy, and the gravitational lensing [3–5]. Also, the DM can be exploited as a solution of well-known problems of modern physics (e.g., the anomalous magnetic moment puzzle [6], large-scale structures [7], etc). Moreover, about $\simeq 85\%$ the total amount of matter in our Universe is approximately invisible, although the fundamental particle nature of DM still remains the great mystery [8, 9]. Thus, the assumption of the dark matter existence motivates the development of SM extensions.

The interaction between SM particles and sub-GeV DM in the thermal bath of the early Universe leads to overproduction of DM particles that require a depletion mechanism to yield the observed density of DM [10–12]. Specifically, an additional connection between DM and SM particles via mediator (MED) as a new portal can lead to observed relic abundance of DM. For example, typical scenarios of DM and the corresponding thermal targets involving dark boson mediators encompass particles with spin-0 [13–19], spin-1 [20–31], and spin-2 [32–43].

Current and planned fixed-target experiments can provide the constraints on Dirac and scalar DM [44], implying the effective interaction between the tensor mediator and (dark) matter. In the present paper, we fill the gap in the literature dedicated to the bremsstrahlung-like production of spin-2 hidden particle in the lepton

fixed-target experiments. In particular, we study the implication of the WW approximation for calculating the cross section of tensor-mediator production in various accelerator-based experiments.

To be more specific, we continue the study of authors of Refs. [19, 45–49] and calculate the production cross sections of spin-2 DM mediator by using the exact-tree-level (ETL) and WW methods for NA64e, NA64 μ , LDMX, and M³ experiments. The implication of the WW approximation [50–53] for spin-0 and spin-1 MED has been investigated for: (i) a electron mode of the E137 experiment [46, 47], (ii) a muon mode in the case of NA64 μ [19, 48], and (iii) a proton bremsstrahlung [54–60].

In addition, we calculate the experimental sensitivity of E137 and LDMX involving visible decays of spin-2 DM mediator in the mass range of interest, $100 \text{ MeV} \lesssim m_G \lesssim 1 \text{ GeV}$. That benchmark simplified scenario implies the universal coupling of spin-2 particle with the charged leptons and photon.

Our study might be complementary to Refs. [43, 61], that explicitly discussed the accelerator-based bounds on photon-specific spin-2 DM mediator. We note that authors of Refs. [33, 35, 62] consider explicitly the ultra violet completion for the scenarios of spin-2 DM mediator in the context of the warped extra dimension and discuss the thermal production mechanisms for dark matter with various channels and the dark matter self-scattering. The latter analysis is beyond the scope of the present paper, in our study we just adopt the DM relic abundance curves from [33] for vector, scalar and Dirac DM, that are complementary to the sensitivity of E137, implying simplified massive spin-2 DM mediator scenario.

In Sec. II we discuss the benchmark models of the spin-2 mediator and main parameters of the considered lepton fixed-target experiments. In Sec. III we briefly describe the procedure of cross section calculation in the case of bremsstrahlung-like production of mediator at lepton fixed-target experiments and derive the corre-

* e-mail: i.v.voronchikhin@gmail.com

† e-mail: dmbriick@gmail.com

sponding matrix elements. In Sec. IV we discuss the differential and total cross sections for the tensor mediator and lepton fixed-target experiments. In Sec. V we discuss the number of signal events and derive the experimental reach of E137 and LDMX in the visible mode. We conclude in Sec. VI. In Appendices A and B we collect some helpful formulas.

II. BENCHMARK SCENARIOS AND EXPERIMENTS

A. Model of mediator

Effective Lagrangian density of the massive spin-2 mediator and matter reads as [32, 33, 63]:

$$\mathcal{L}_{\text{eff}}^G \supset - \sum_i c_i^G G^{\mu\nu} T_{\mu\nu}^i, \quad (1)$$

where $T_{\mu\nu}^i$ is the energy-momentum tensor (EMT) and $c_i^G = (c_{\text{DM}}^G, c_{\text{SM}}^G)$ is a coupling constant of dimension GeV^{-1} between the massive spin-2 mediator and corresponding types of (dark) matter.

In the cases of scalar, S , vector, V^μ , and Dirac fermion, ψ , types of massive DM particles, the symmetrized EMTs read, respectively [33]:

$$T_{\mu\nu}^S = \partial_\mu S \partial_\nu S - (1/2) \eta_{\mu\nu} [(\partial_\rho S)^2 - m_S^2 S^2], \quad (2)$$

$$T_{\mu\nu}^V = (1/4) \eta_{\mu\nu} V_{\lambda\rho} V^{\lambda\rho} - V_{\mu\lambda} V^\lambda{}_\nu + m_V^2 V_\mu V_\nu - (1/2) m_V^2 \eta_{\mu\nu} V_\alpha V^\alpha, \quad (3)$$

$$T_{\mu\nu}^\psi = -(i/4) \bar{\psi} \left[\gamma_\mu \overleftrightarrow{\partial}_\nu + \gamma_\nu \overleftrightarrow{\partial}_\mu \right] \psi + \eta_{\mu\nu} m_\psi \bar{\psi} \psi + (i/2) \eta_{\mu\nu} \bar{\psi} \gamma^\rho \overleftrightarrow{\partial}_\rho \psi, \quad (4)$$

where we denote $\bar{\psi} \overleftrightarrow{\partial}_\mu \psi = (\partial_\mu \bar{\psi}) \psi - \bar{\psi} (\partial_\mu \psi)$ and $m_{\text{DM}} = (m_S, m_V, m_\psi)$ is a mass of the corresponding DM type. Next, the EMT of SM particles reads as [63]:

$$T_{\mu\nu}^{\text{SM}} = \left[\frac{1}{4} \eta_{\mu\nu} F_{\lambda\rho} F^{\lambda\rho} - F_{\mu\lambda} F^\lambda{}_\nu \right] - \frac{i}{4} \bar{l} \left[\gamma_\mu \overleftrightarrow{D}_\nu + \gamma_\nu \overleftrightarrow{D}_\mu \right] l + \frac{i}{2} \eta_{\mu\nu} \bar{l} \gamma^\rho \overleftrightarrow{D}_\rho l, \quad (5)$$

where l is the SM lepton, $F_{\mu\nu} = \partial_\mu A_\nu - \partial_\nu A_\mu$ is the strength tensor for the SM photon field A_μ , $D_\mu = \partial_\mu - ieA_\mu$ is the covariant derivative for the $U(1)$ gauge field, we use notation $\bar{l} \overleftrightarrow{D}_\mu l = (D_\mu^* \bar{l}) l - \bar{l} (D_\mu l)$.

The spin-2 vertices involving fermion, vector and scalar

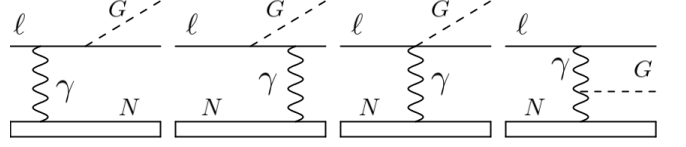


Figure 1. Feynman diagrams describing bremsstrahlung-like signature for the tensor mediator. Typically, one can consider two benchmark scenarios for spin-2 DM mediator [33]. It can decay either to the pair of SM particles, $G \rightarrow \text{SM} + \text{SM}$, or to the invisible DM sector, $G \rightarrow \text{DM} + \text{DM}$, implying its branching fraction is $\text{Br}(G \rightarrow \text{DM} + \text{DM}) \simeq 1$.

	NA64e	LDMX	NA64μ	M ³	E137
target material	Pb	Al	Pb	W	Al
Z, atomic number	82	13	82	74	13
A, g · mole ⁻¹	207	27	207	184	27
$x_{\text{cut}} = E_{\text{G}}^{\text{cut}}/E_l$	0.5	0.7	0.5	0.4	0.1
l^\pm , primary beam	e	e	μ	μ	e
E_l , GeV, beam energy	100	16	160	15	20
vis. mode, $G \rightarrow \text{SM} + \text{SM}$	+	+	-	-	+
inv. mode, $G \rightarrow \text{DM} + \text{DM}$	+	+	+	+	-

Table I. The benchmark parameters for the spin-2 mediator production cross section $l^\pm N \rightarrow l^\pm N + G$ at the lepton fixed-target experiments. Note that the $E_{\text{G}}^{\text{cut}} = x_{\text{cut}} E_l$ is a typical minimum missing energy threshold that is associated with the specific fixed-target facility.

field in the momentum space read as, respectively:

$$T_{\mu\nu}^{(Gff)}(p_1, p_2) = (-ic_{ff}^G)/4 \left[\gamma_\mu (p_1 + p_2)_\nu + \gamma_\nu (p_1 + p_2)_\mu - 2\eta_{\mu\nu} (\not{p}_1 + \not{p}_2 - 2m_f) \right], \quad (6)$$

$$T_{\mu\nu\alpha\beta}^{(GVV)}(k_1, k_2) = (-ic_{VV}^G) \left[m_V^2 C_{\mu\nu\alpha\beta} + (C_{\mu\nu\alpha\beta\sigma\lambda} + C_{\nu\mu\alpha\beta\sigma\lambda}) k_1^\sigma k_2^\lambda \right], \quad (7)$$

$$T_{\mu\nu}^{(GSS)}(q_1, q_2) = (-ic_{SS}^G) [\eta_{\mu\nu} m_S^2 - q_1^\alpha q_2^\beta C_{\mu\nu\alpha\beta}], \quad (8)$$

where p_1, p_2 are 4-momenta of fermions, k_1, k_2 are 4-momenta of vector particles $V_\alpha(k_1)$ and $V_\beta(k_2)$, q_1, q_2 are 4-momenta of scalar particles, in Eqs. (7) and (8) we use the following notations:

$$C_{\mu\nu\alpha\beta} = (\eta_{\mu\alpha} \eta_{\nu\beta} + \eta_{\nu\alpha} \eta_{\mu\beta} - \eta_{\mu\nu} \eta_{\alpha\beta}),$$

$$C_{\mu\nu\alpha\beta\sigma\lambda} = \frac{1}{2} \eta_{\mu\nu} (\eta_{\beta\sigma} \eta_{\alpha\lambda} - \eta_{\sigma\lambda} \eta_{\alpha\beta}) + \eta_{\alpha\beta} \eta_{\mu\sigma} \eta_{\nu\lambda} - \eta_{\mu\beta} \eta_{\nu\sigma} \eta_{\alpha\lambda} + \eta_{\mu\alpha} (\eta_{\beta\nu} \eta_{\sigma\lambda} - \eta_{\sigma\beta} \eta_{\lambda\nu}).$$

In addition, the 4-legs vertex reads:

$$T_{\mu\nu\alpha}^{(Gll\gamma)} = (-e/2) (-ic_{ll}^G) [\eta_{\alpha\nu} \gamma_\mu + \eta_{\mu\alpha} \gamma_\nu - 2\eta_{\mu\nu} \gamma_\alpha]. \quad (9)$$

The Feynman diagrams are shown in Fig. 1 for the bremsstrahlung-like production of spin-2 mediator.

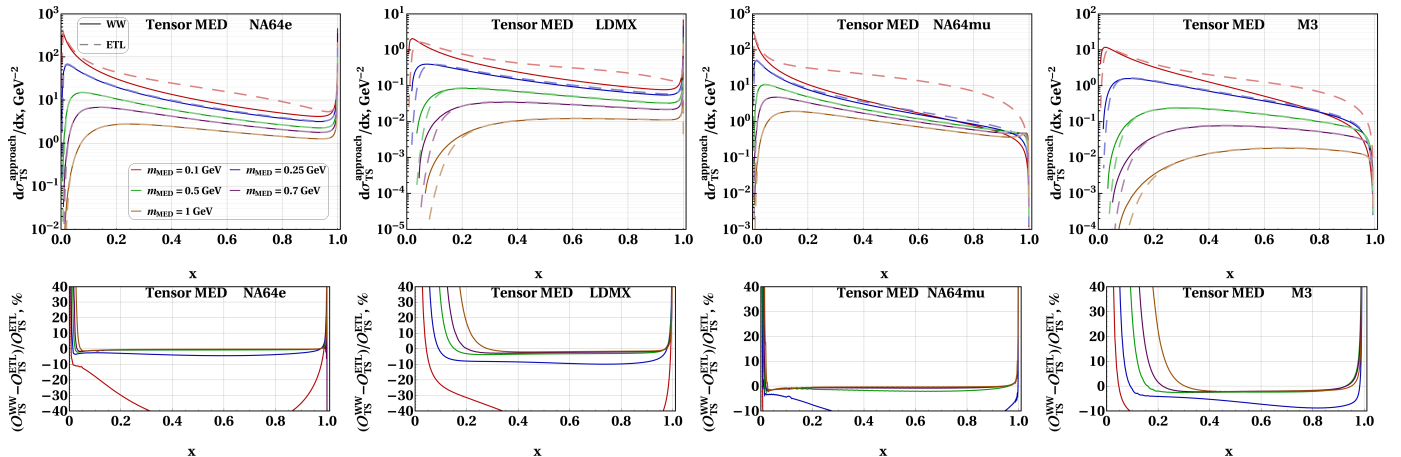


Figure 2. The differential cross sections as a function of energy fraction x in the case of tensor mediator for different approximations and the corresponding relative difference, where the columns correspond to NA64e, LDMX, NA64 μ , and M³ experiments, respectively. We also set $\theta_{\max} = 0.1$ and $c_{li}^G = 1 \text{ GeV}^{-1}$. The curve colors correspond to fixed values of the mediator masses. In the upper row we show the differential cross sections for different masses, where the solid and dashed lines correspond to the WW and ETL approximations, respectively. In the bottom row the relative difference of differential cross sections between the WW and ETL approximations are shown.

B. The experiments to search for the invisible decays of MED

The mediator of DM can be produced in bremsstrahlung-like process where a lepton beam with the initial energy E_l incidents on a fixed target. In particular, the fraction $x = E_{\text{miss}}/E_l$ of the primary beam energy E_l can be carried away in dark sector that leads to a missing energy deposition in a detector system. That can imply the invisible decay of spin-2 mediator into DM particles, with $\text{Br}(G \rightarrow \text{DM} + \text{DM}) \simeq 1$. Moreover, the fixed-target experiments can probe the parameter space of light DM due to a high-energy particle beam and its relative large intensity. In Tab. I the crucial parameters of the considered fixed-target experiments are shown. *NA64e*: the experiment is located in the north area of the European Organization for Nuclear Research (CERN) on the H4 line of the super proton synchrotron (SPS) [64]. *NA64 μ* : this experiment corresponds to the muon beam mode at the M2 line of the SPS in the north area of CERN, which uses the detector system structure of the NA64e experiment [65]. *LDMX*: the Light Dark Matter Experiment is a planned experiment with an electron beam at Stanford Linear Accelerator Center (SLAC) in which missing energy signatures are complemented by a unique technique to measure the missing momentum of electrons [66, 67]. *M³*: this detector is considered as complementary part of the LDMX, it has a similar detector base [68] and involves a muon beam.

III. BREMSSTRAHLUNG-LIKE PRODUCTION OF THE TENSOR MEDIATOR

The radiation of a dark matter mediator by a lepton scattering off a heavy nucleus can be represented as a $2 \rightarrow 3$ process:

$$l^\pm(p) + N(P_i) \rightarrow l^\pm(p') + N(P_f) + G(k), \quad (10)$$

where $p = (E_l, \mathbf{p})$, $p' = (E'_l, \mathbf{p}')$ are 4-momenta of the incoming and outgoing leptons, respectively, $k = (E_G, \mathbf{k})$ is 4-momentum of the dark matter mediator, $P_i = (M, 0)$ and $P_f = (P_f^0, \mathbf{P}_f)$ are 4-momenta of the initial and final nucleus, respectively, $q = (q_0, \mathbf{q}) \equiv P_i - P_f$ is 4-momentum transferred to the nucleus, and virtuality of the photon is $t \equiv -q^2 = -(P_i - P_f)^2$. The Mandelstam-like variables for the process (10) can be introduced as:

$$\begin{aligned} \tilde{s} &= (p' + k)^2 - m_l^2, & \tilde{u} &= (p - k)^2 - m_l^2, \\ \tilde{t} &= (p - p')^2 - m_G^2. \end{aligned} \quad (11)$$

In general, the interaction of an electromagnetic field A_μ and a hadron can be effectively represented as [69]:

$$\mathcal{L}_{\text{eff}}^{\text{nucl}} \supset -eA_\mu \mathcal{J}^\mu, \quad (12)$$

where \mathcal{J}^μ is a hadronic current [70, 71]. For heavy nucleus one can exploit a spin-0 form-factor with a good accuracy [72]. Thus, the hadronic current in the momentum space reads as follows [72, 73]:

$$\mathcal{J}^\mu = F(t)(P_f + P_i)^\mu. \quad (13)$$

The nuclear form-factor in the laboratory frame is associated with charge density of nucleus through the Fourier transformation [48, 74, 75]. The elastic atomic Tsai-

Schiff's [75, 76] form-factor takes the following form:

$$F_{\text{TS}}(t) = \frac{t}{t_a + t} \frac{t_d}{t_d + t}, \quad (14)$$

where $\sqrt{t_d} = 0.164A^{-1/3}\text{GeV}$ is the typical momentum associated with the effective nuclear radius, R_n , such that $t_d = 1/R_n^2$ and $\sqrt{t_a} = 1/R_a$ is typical momentum associated with the atomic radius, $R_a = 111Z^{-1/3}/m_e$. Also, we take into account that $|\mathbf{q}| \lesssim \mathcal{O}(100)$ MeV and $M \propto \mathcal{O}(100)$ GeV imply the relation $|\mathbf{q}|/M \ll 1$.

The matrix element for the process (10) can be written as:

$$i\mathcal{M}_{2 \rightarrow 3}^{\text{G}} = ic_{ll}^{\text{G}} e^2 \mathcal{L}^\mu \left(\frac{-i\eta_{\mu\nu}}{q^2} \right) \mathcal{J}^\nu = iC_{\mathcal{M}} \mathcal{L}^\mu P_\mu, \quad (15)$$

where we denote $C_{\mathcal{M}} = c_{ll}^{\text{G}} e^2 F_s(q^2)/q^2$ and $P^\mu = (P_f + P_i)^\mu$. The corresponding lepton current $\mathcal{L}^\mu = \sum_{i=1}^4 (\mathcal{L}_i)^\mu$ with mediator radiation consists of the terms:

$$(\mathcal{L}_1)_\lambda = -i\varepsilon^{*\mu\nu}(k) \cdot \bar{u}(p') T_{\mu\nu}^{(\text{G}ll)}(p' + k, p') \frac{\not{p}' + \not{k} + m_l}{\tilde{s}} \gamma_\lambda u(p), \quad (16)$$

$$(\mathcal{L}_2)_\lambda = -i\varepsilon^{*\mu\nu}(k) \cdot \bar{u}(p') \gamma_\lambda \frac{\not{p} - \not{k} + m_l}{\tilde{u}} T_{\mu\nu}^{(\text{G}ll)}(p, p - k) u(p), \quad (17)$$

$$(\mathcal{L}_3)_\lambda = -i\varepsilon^{*\mu\nu}(k) \bar{u}(p') \left(T_{\mu\nu\lambda}^{(\text{G}l\gamma)} / e \right) u(p), \quad (18)$$

$$(\mathcal{L}_4)_\lambda = +i\varepsilon^{*\mu\nu}(k) \cdot T_{\mu\nu\beta\lambda}^{(\text{G}\gamma\gamma)}(p - p', q) \bar{u}(p') \frac{\gamma^\beta}{\tilde{t} + m_G^2} u(p). \quad (19)$$

The the matrix element squared for the process $2 \rightarrow 3$ can be written as:

$$|\mathcal{M}_{2 \rightarrow 3}^{\text{G}}|^2 = C_{\mathcal{M}}^2 |\mathcal{A}_{2 \rightarrow 3}^{\text{G}}|^2, \quad (20)$$

where the expression for the effective mediator production amplitude squared $|\mathcal{A}_{2 \rightarrow 3}^{\text{G}}|^2$ is shown in appendix B.

The ETL double differential cross section for the bremsstrahlung-like production of mediator takes the following form [46, 47]:

$$\frac{d\sigma_{2 \rightarrow 3}}{dx d\cos(\theta_G)} = \frac{(c_{ll}^{\text{G}})^2 \alpha^3 Z^2}{4\pi} \frac{|\mathbf{k}| E_p}{|\mathbf{P}| |\mathbf{k} - \mathbf{p}|} \cdot \int_{t_{\min}}^{t_{\max}} dt \frac{F^2(t)}{t^2} \frac{1}{8M^2} \int_0^{2\pi} \frac{d\phi}{2\pi} |\mathcal{A}_{2 \rightarrow 3}^{\text{G}}|^2, \quad (21)$$

where $\alpha = e^2/(4\pi) \simeq 1/137$ is the fine structure constant, $x = E_G/E_l$ is the fraction of the total energy of the mediator with respect to the energy of original lepton, $t_{\max} = t(Q_+)$ and $t_{\min} = t(Q_-)$ are the maximum and minimum squares of the 4-momentum and are introduced notations:

$$Q_\pm = \left| \frac{|\mathbf{V}| [\tilde{u} + 2M(M - V_0)] \pm (M - V_0) \sqrt{D_0}}{2(M - V_0)^2 - 2|\mathbf{V}|^2} \right|,$$

$$V \equiv k - p, \quad D_0 = 4M^2 |\mathbf{V}|^2 + \tilde{u}^2 + 4M d_{V_0} \tilde{u}.$$

The double differential cross section in the WW approximation takes the following form [75, 77]:

$$\left. \frac{d\sigma(p + P_i \rightarrow p' + P_f + k)}{d(pk) d(kP_i)} \right|_{\text{WW}} = \frac{\alpha\chi}{\pi(p'P_i)} \left. \frac{d\sigma(p + q \rightarrow k + p')}{d(pk)} \right|_{t=t_{\min}}. \quad (22)$$

where the differential cross section for the Compton-like process

$$l^\pm(p) + \gamma(q) \rightarrow l^\pm(p') + G(k), \quad (23)$$

can be written as:

$$\frac{d\sigma(p + q \rightarrow k + p')}{d(pk)} = \frac{(c_{ll}^{\text{G}})^2 e^2 |\mathcal{A}_{2 \rightarrow 2}^{\text{G}}|^2}{8\pi(s_2 - m_l^2)^2}, \quad (24)$$

where $|\mathcal{A}_{2 \rightarrow 2}^{\text{G}}|^2$ is the amplitude squared of the Compton-like processes [44].

The flux of virtual photon χ from nucleus in Eq. (22) is expressed through the elastic form-factor $F(t)$ as follows:

$$\chi = Z^2 \int_{t_{\min}}^{t_{\max}} \frac{t - t_{\min}}{t^2} F^2(t) dt. \quad (25)$$

The minimum value of virtuality in WW approximation t_{\min}^{WW} reads:

$$t_{\min}^{\text{WW}} \simeq U^2 / (4E_l^2 (1 - x)^2), \quad (26)$$

where we denote the following function:

$$U \equiv m_l^2 - u_2 \simeq E_l^2 \theta_G^2 x + m_G^2 (1 - x) / x + m_l^2 x > 0. \quad (27)$$

In the so-called improved WW (IWW) approach [45, 47] the dependence of t_{\min} on x and θ_G in the flux derivation is omitted to simplify calculations, which is important for the integration that exploits, for instance, Monte-Carlo (MC) methods [48], such that

$$t_{\min}^{\text{IWW}} \simeq m_G^4 / (4E_l^2).$$

Using Jacobian of the transformation from (k, p) and (k, P_i) to $\cos(\theta_G)$ and $x = E_G/E_l$ variables in the case of a ultra-relativistic incident lepton in laboratory frame, one can get:

$$\left. \frac{d\sigma(p + P_i \rightarrow p' + P_f + k)}{dx d\cos(\theta_G)} \right|_{\text{WW}} = \frac{\alpha\chi}{\pi} \cdot \frac{E_l^2 x \beta_G}{1 - x} \left. \frac{d\sigma(p + q \rightarrow k + p')}{d(pk)} \right|_{t=t_{\min}}, \quad (28)$$

where $\beta_G = \sqrt{1 - m_G^2/(xE_l)^2}$ is the typical velocity of mediator.

IV. THE BREMSSTRAHLUNG-LIKE CROSS SECTIONS

In this section, we compare the cross sections in the WW and ETL approaches for fixed-target experiments. The total and differential cross sections are calculated

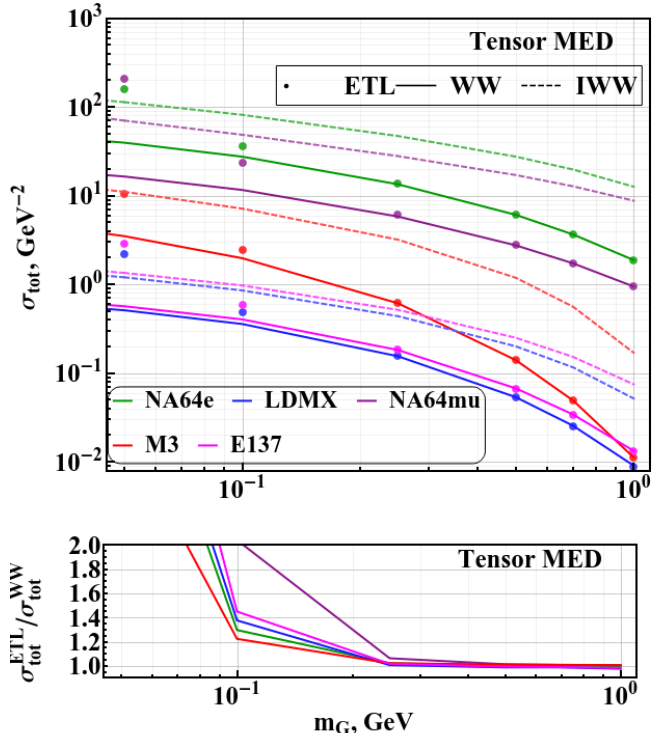


Figure 3. The total cross sections σ_{tot} for tensor mediator production with typical angle cut $\theta_{\text{max}} = 0.1$, where the benchmark Tsai-Schiff’s form-factor is chosen. The green, blue, purple, red and magenta lines correspond to NA64e, LDMX, NA64 μ , M³, and E137 experiments, respectively. Solid line, dashed line and dots correspond to calculations for WW, IWW, and ETL approximations, respectively.

by the numerical integration of the amplitude squared over the phase space for the specific experimental setup. Moreover, Tsai-Schiff’s form-factor (14) is used as a benchmark one for the cross section in the WW and ETL approach [48, 74, 78, 79] throughout the paper.

We note that the impact of different form-factors parametrization on cross section was studied in Ref. [44, 49]. An optimal value of the maximum angle of G-emission is chosen to be $\theta_{\text{max}} \simeq 0.1$, since the dominant contribution to the cross section occurs in the peak-forward region [49, 80, 81].

A. The differential cross section for invisible mode experiments

In this section, we discuss only experiments that aim to the search for the invisible mode decay of tensor mediator (see e. g. Tab. I). In Fig. 2 we show WW and ETL differential cross sections for the specific parameter set and the comparison between the corresponding approaches.

To be more specific, the relative difference between the WW and ETL differential cross sections for various

experiments can be described as follows. *NA64e*: For the relatively large masses $m_G \gtrsim 100$ MeV, the using of WW approximation leads to overestimation at the level of $\mathcal{O}(10)$ % around $x \simeq 1$ and $x \ll 1$, the discrepancy is negligible, $\lesssim \mathcal{O}(1)$ %, for intermediate energy fraction range $x \lesssim 1$. However, for masses $m_G \lesssim 100$ MeV, WW approximation leads to underestimation at the level of $\gtrsim \mathcal{O}(10)$ % for the intermediate values $x \lesssim 1$. *NA64 μ* : The relative difference for that one is similar to the NA64e case, although a sizable discrepancy, $\gtrsim \mathcal{O}(50)$ %, appears for the masses $m_G \lesssim 200$ MeV. *LDMX* and *M³*: the behavior of the relative differences is similar to the shapes of NA64e and NA64 μ , respectively, however the $\mathcal{O}(10)$ % overestimation for the heavy masses, $m_G \gtrsim 100$ MeV, occurs in the intermediate range $x \lesssim 1$.

It is important to emphasize that for a tensor mediator with masses $m_G \gtrsim 100$ MeV one has a fairly well agreement between the differential cross sections calculated in the WW and the ETL, for all experiments of interest. However, a sizable difference, $\gtrsim \mathcal{O}(50)$ %, between corresponding approaches arises due to the rapid increasing of the differential cross section for small mass range $m_G \lesssim 100$ GeV. Indeed, the $lN \rightarrow lNG$ amplitude squared in the ETL method (see e. g. Eq. (B1)) includes the typical terms of negative mass power, $\propto 1/m_G^2$ and $\propto 1/m_G^4$, that arise due to the summation over longitudinal polarizations (A4) of the light spin-2 mediator. For the $l\gamma^* \rightarrow lG$ amplitude squared in the WW the regarding mass terms are absent, see Ref. [39, 44]. As a result, in the ETL cross section for relatively large masses $m_G \gtrsim 100$ MeV, the typical terms $\propto 1/m_G^2$ and $\propto 1/m_G^4$ can be negligible with the respect to the terms of $\propto m_G^0$, $\propto m_G^2$, $\propto m_G^4$, etc. Such that, the differential cross sections for both the WW and the ETL methods are in a good agreement, implying the the intermediate energy fraction range, $x \lesssim 1$.

We note that the typical shape of the relative difference between the WW and ETL differential cross sections for tensor-mediator masses $m_G \gtrsim 100$ MeV is similar to the one calculated for the spin-0 and spin-1 mediators (see e. g. Ref. [49] for detail).

To conclude this sub-section we note that the differential cross section and the corresponding relative difference in ETL and WW calculations are similar for both the E137 and the LDMX experiments. These experiments have a similar target and beam energy parameters, which are given in the Tab. IIB.

B. The total cross section

In Fig. 3 we show the total cross section as a function of m_G and the regarding ration between the WW and ETL approach for benchmark fixed-target experiments presented in Tab. I. That implies the typical benchmark angle cut $\theta_{\text{max}} = 0.1$. For relatively large masses $m_G \gtrsim 200$ MeV, the relative difference between two approaches is at the level of $\mathcal{O}(1)$ %, however relative dif-

ference can reach $\mathcal{O}(20)$ % for the tensor-mediator mass range below $m_G \lesssim 100$ MeV.

The origin of discrepancy in the small mass region is discussed in Sec. IV A, i. e. it can also be referred to the typical $\propto 1/m_G^2$ and $\propto 1/m_G^4$ terms that arise in the ETL amplitude squared for the process $lN \rightarrow lNG$.

We address the typical range of the large masses $m_G \gtrsim 200$ MeV as a region of robust calculation, for which WW and ETL approaches yield fairly good agreement. That can be crucial for the fixed-target experiments [44, 82] that search for the bremsstrahlung-like production of the tensor mediator, $lN \rightarrow lNG$, followed by its invisible decay into pair of DM particles, $G \rightarrow \text{DM} + \text{DM}$. The regarding sensitivities to the invisible mode of G can be found elsewhere Refs. [44, 82], that implies WW approach for the G-strahlung cross section calculation.

In the next section, we focus on the visible mode decay of the light spin-2 mediator into pair of SM particles, $G \rightarrow \gamma\gamma(e^+e^-)$, that exploits the results of the present section.

V. VISIBLE MODE

If the dark matter is heavier than its mediator, $m_G \lesssim 2 m_{\text{DM}}$, then the corresponding mediator can only decay into SM particles due to the kinematical conditions. A signal in visible mode means that the mediator passes through the target and decays before the detector system. The corresponding thermal curves for the tensor mediator can be found in the Ref. [33], implying that the DM consists of scalar, vector, or Dirac particles. Remarkably, the E137 experiment [83] can yield a new constraint for the tensor mediator due to the large collected statistics, where the spin-2 mediator visibly decays into $G \rightarrow \gamma\gamma$ and $G \rightarrow e^+e^-$ in the mass range $m_G \gtrsim \mathcal{O}(100)$ MeV. In what follows, we consider the spin-2 mediator, which predominantly couples to photons and electrons [33].

A. The experiments to search for the visible decays of the tensor mediator

E137: The experiment E137 at Stanford Linear Accelerator Center (SLAC) was originally designed to search for axion-like particles as neutral metastable particles [83]. The null-result of E137 experiment can be exploited to set constraints on parameter space of spin-2 boson. Particles of hidden sector can be produced by a 20 GeV electron beam incident on a fixed target that consists of a set of aluminum plates interlaced with cooling water. The mediator produced by G-strahlung reaction can pass 179 m of shielding and decay on 204 m long open region before a detector. In particular, the detector of E137 experiment consists of an 8-radiation length electromagnetic shower calorimeter that can detect charged par-

ticles or photons produced by the mediator. For the E137 experiment the electrons accumulated on target (EOT) are set to be at the level of $\text{EOT} = 1.87 \times 10^{20}$.

LDMX: We also discuss for completeness the LDMX expected reach for the visible mode, the corresponding experimental parameters are provided in Section II B. We set the expected statistics of the LDMX to be $\text{EOT} = 10^{15}$.

B. Signal events for visible mode

The cut for the mediator energy ratio $x_{\text{cut}} = E_G^{\text{cut}}/E_l$ is used in order to specify the typical missing energy signature of the considered fixed-target experiments (see e. g. Tab. I). Note that the total cross section of bremsstrahlung-like tensor-mediator production for the specific experiment is:

$$\sigma_{\text{tot}}(E_e) = \int_{x_{\text{cut}}}^1 dx \int_0^{\theta_{\text{max}}} d\theta_G \frac{d\sigma_{2 \rightarrow 3}}{dx d\theta_G}(E_e),$$

where the double differential cross section is shown in Sec. III for various approaches, θ_G is an angle between initial beam direction and momentum of the produced G.

Assuming production of a mediator in the first radiation length, one can estimate the number of the bremsstrahlung-like mediator production for fixed-target facilities as follows [84]:

$$N_G^{\text{brem.}} \simeq \text{EOT} \cdot \frac{\rho N_A}{A} L_T \cdot \sigma_{\text{tot}}(E_e), \quad (29)$$

where $X_0 = 8.9$ cm is a radiation length of the aluminium, $L_T^{\text{LDMX}} \simeq 0.4X_0$, $L_T^{\text{E137}} \simeq X_0$ are effective radiation lengths of the LDMX and E137 experiments, respectively. The decay length of the new particle in the lab frame is:

$$l_G = \frac{E_G}{m_G} \frac{1}{\Gamma_G^{\text{tot}}}, \quad (30)$$

where Γ_G^{tot} is a total decay width $\Gamma_G^{\text{tot}} = \Gamma_{G \rightarrow ee} + \Gamma_{G \rightarrow \gamma\gamma}$ with $\Gamma_{G \rightarrow ee}$ and $\Gamma_{G \rightarrow \gamma\gamma}$ being a partial decay widths to the electron and the photon, respectively [32]:

$$\Gamma_{G \rightarrow ee} = \frac{(c_{ee}^G)^2 m_G^3}{160\pi} \left(1 + \frac{8}{3} \frac{m_e^2}{m_G^2}\right) \left(1 - 4 \frac{m_e^2}{m_G^2}\right)^{3/2}, \quad (31)$$

$$\Gamma_{G \rightarrow \gamma\gamma} = 13 \frac{(c_{\gamma\gamma}^G)^2 m_G^3}{960\pi}. \quad (32)$$

The coupling constants are chosen to be $c_{\gamma\gamma}^G = c_{ee}^G$. For the decay length into photons, one can get:

$$l_{G \rightarrow \gamma\gamma} \simeq 4.5 \cdot 10^5 \text{ cm} \times \left(\frac{E_G}{10 \text{ GeV}}\right) \left(\frac{0.1 \text{ GeV}}{m_G}\right)^4 \left(\frac{10^{-6} \text{ GeV}^{-1}}{c_{ee}^G}\right)^2.$$

Next, using the thick target approximation, the number of signal event in visible mode takes the following

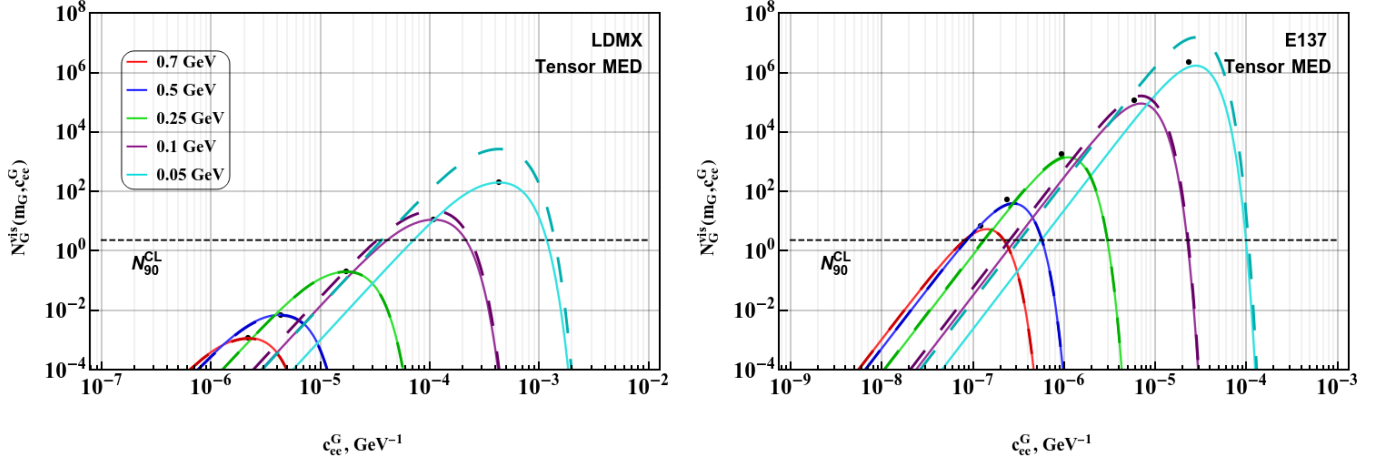


Figure 4. Number of signal events (33) as a function of the coupling constant c_{ee}^G for the typical set of masses. Left and right panels correspond to the LDMX (EOT = 10^{15}) and E137 (EOT = 1.87×10^{20}). The number of signal events for the ETL (21) and WW (28) methods corresponds to the dashed and solid lines, respectively.

form [85]:

$$N_G^{\text{vis.}} \simeq N_G^{\text{brem.}} \times (e^{-L_{\text{sh}}/l_G} - e^{-L_{\text{tot}}/l_G}), \quad (33)$$

where L_{sh} is the length of shield, $L_{\text{tot}} = L_{\text{sh}} + L_{\text{dec}}$ with L_{dec} being the length of the fiducial volume. In Eq. (33) we suppose that the dominant part of the electron energy transfers to the tensor mediator, such that $E_e \simeq E_G$. The signals from secondary positrons production in the target [86] and the absorption processes [47] are neglected in our calculation. The shielding parameters for LDMX [85] and E137 [47, 87] read, respectively:

$$L_{\text{sh}}^{\text{LDMX}} = 43 \text{ cm}, \quad L_{\text{tot}}^{\text{LDMX}} = 315 \text{ cm}, \quad (34)$$

$$L_{\text{sh}}^{\text{E137}} = 179 \text{ m}, \quad L_{\text{dec}}^{\text{E137}} = 204 \text{ m}. \quad (35)$$

In Fig. 4 we show the number of signal events for LDMX and E137 experiments.

C. The experimental limits

Assuming background free case and zero signal events observed at fixed-target experiments we require 90 %C. L. upper limit on the number of spin-2 mediator decays to be $N_{90\%}^{\text{CL}} \simeq 2.3$ according to Poisson statistics. For each mediator mass m_G , the range of coupling constrained $c_{ee}^{\text{low}}(m_G) \lesssim c_{ee}^G \lesssim c_{ee}^{\text{up}}(m_G)$ is defined by inequality $N_G^{\text{vis.}} \gtrsim N_{90\%}^{\text{CL}}$, see Fig. 4. The values above $c_{ee}^{\text{up}}(m_G)$ correspond to short-lived decaying before the shield escaping. The values below c_{ee}^{low} correspond to too small signal yield of G decaying beyond the fiducial volume.

In Fig. 5 we show the 90% C.L. sensitivity region of both LDMX and E137 experiments in the G-parameters space for the background free case. These results demonstrate that the E137 experiment has been ruled out the the parameter space of spin-2 DM mediator at the level of $8 \times 10^{-8} \text{ GeV}^{-1} \lesssim c_{ee}^G \lesssim 10^{-5} \text{ GeV}^{-1}$ for the typical

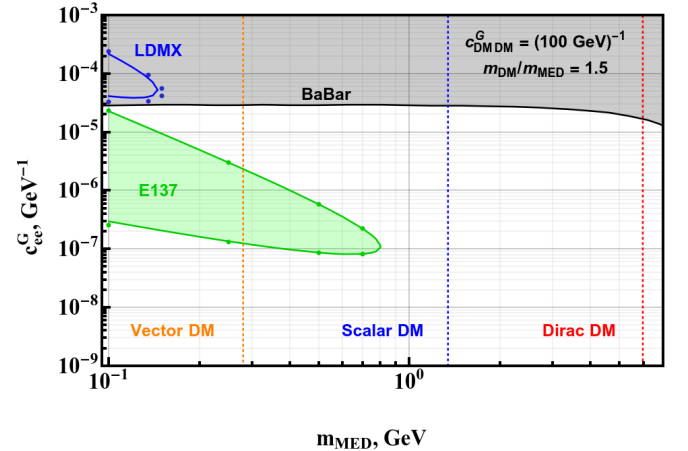


Figure 5. The experimental reach at 90% C.L. as the function of MED mass for the LDMX (EOT = 10^{15}) and E137 (EOT = 1.87×10^{20}) fixed-target facilities in the case of the visible mode. Green shaded region is the current reach of the electron beam dump E137 [83] experiment, and the blue area corresponds to the planned sensitivity of the LDMX experiment. Gray shaded region is the current constraint of BaBar experiment [33]. The relic DM density is shown by the orange, red and blue dashed lines for vector, fermion and scalar DM, respectively [33], also all these lines imply $c_{\text{DM DM}}^G \simeq (100 \text{ GeV})^{-1}$ and $m_{\text{DM}} = 1.5 m_G$. The constraints on the coupling constant using ETL in the case of E137 and LDMX experiments calculations are shown by green and blue dots, respectively.

masses in the range $100 \text{ MeV} \lesssim m_G \lesssim 800 \text{ MeV}$, that corresponds to the EOT = 1.87×10^{20} . The bounds of the LDMX experiment for EOT = 10^{15} have been already ruled out by BaBar data on mono-photon, $e^+e^- \rightarrow G\gamma$, searches for the spin-2 DM mediator. The regarding

lepton collider bound applies to the typical parameter space of the spin-2 mediator with $m_G \lesssim 7$ GeV and $c_{ee}^G \lesssim 3 \times 10^{-5}$ GeV.

In addition we note that the thermal production mechanism of DM involving spin-2 mediator have been analyzed in detail in Ref. [33]. To be more specific, in Fig. 5 we show the typical relic-abundance curves for the scalar, vector and Dirac DM adapted from Ref. [33]. These lines imply the typical DM couplings $c_{SS}^G = c_{\psi\psi}^G = c_{VV}^G = 10^{-2}$ GeV $^{-1}$ and benchmark mass ratio $m_{DM}/m_G = 1.5$, that leads to the visible decays of spin-2 mediator. Remarkably, the E137 experiment has been ruled out the vector DM with $m_V \simeq 300$ MeV for the coupling constant in the range 10^{-7} GeV $^{-1} \lesssim c_{ee}^G \lesssim 3 \times 10^{-6}$ GeV $^{-1}$. In addition, we note that E137 searches are not sensitive to both scalar and Dirac DM.

VI. CONCLUSION

In the present paper, we have discussed in detail the calculation of the DM mediator production cross sections in the case of ETL and WW approaches for fixed-target experiments, such as NA64e, LDMX, NA64 μ , and M 3 . Tensor massive particle G is chosen as hidden-sector mediator, that is produced in the bremsstrahlung-like reaction $lN \rightarrow lNG$ followed by its invisible decay into DM pair, $G \rightarrow DM + DM$. Our study shows that for mass range $m_G \gtrsim 200$ MeV the agreement between ETL and WW methods can be at the level of $\lesssim \mathcal{O}(1)$ % for all fixed-target experiments of interest.

In addition, we have studied the properties of the spin-2 particle production in the bremsstrahlung-like reaction $lN \rightarrow lNG$ and its visible decays, $G \rightarrow \gamma\gamma$ and $G \rightarrow e^+e^-$, for the LDMX and E137 experiments. We have calculated the expected sensitivity to spin-2 DM mediator of the LDMX experiment for the statistics EOT = 10^{15} and have shown that the regarding parameter space was ruled out by mono-photon BaBar searches, $e^+e^- \rightarrow G\gamma$. We derived novel constraints of the E137 experiment that are associated with the coupling constant region 10^{-7} GeV $^{-1} \lesssim c_{ee}^G \lesssim 10^{-5}$ GeV $^{-1}$ for the mass range 100 MeV $\lesssim m_G \lesssim 800$ MeV, that corresponds to the statistics of EOT = 1.87×10^{20} electrons

accumulated on target.

VII. ACKNOWLEDGEMENTS

This work is supported by RSF grant no. 24-72-10110. We would like to thank A. Arbuzov, R. Dusaev, D. Gorbunov, S. Gninenko, V. Kim, M. Kirsanov, N. Krasnikov, E. Kriukova, V. Lyubovitskij, S. Ramazanov, A. Shevelev, and A. Zhevlakov for fruitful discussions.

Appendix A: Tensor mediator

We focus on the linearized theory of the massive spin-2 particle [88, 89]:

$$S_{\text{FP}} = \frac{1}{2} \int d^D x [\partial_\sigma G_{\mu\nu} \partial^\sigma G^{\mu\nu} - 2\partial_\mu G_{\nu\sigma} \partial^\nu G^{\mu\sigma} + 2\partial_\mu G^{\mu\nu} \partial_\nu G - \partial_\sigma G \partial^\sigma G - m_G^2 (G_{\mu\nu} G^{\mu\nu} - G^2)], \quad (\text{A1})$$

where $\eta_{\mu\nu}$ is Minkowski metric. Next, by varying the action (A1) over the field $G^{\mu\nu}$, one can obtain the Fierz-Pauli equation for a massive spin-2 particle that takes the following form [90]:

$$\partial_\sigma \partial^\sigma G^{\mu\nu} - \partial_\sigma \partial_\mu G^\sigma{}_\nu - \partial_\sigma \partial_\nu G^\sigma{}_\mu + \eta_{\mu\nu} \partial_\lambda \partial^\lambda G^{\lambda\sigma} + \partial_\mu \partial_\nu G - \eta_{\mu\nu} \partial_\sigma \partial^\sigma G + m_G^2 (G_{\mu\nu} - G) = 0. \quad (\text{A2})$$

After some simplifications, one can get the Klein-Gordon equation, $(\partial_\sigma \partial^\sigma + m_G^2) G_{\mu\nu} = 0$, with additional conditions

$$G_\mu^\mu \equiv G = 0, \quad \partial^\mu G_{\mu\nu} = 0. \quad (\text{A3})$$

By taking into account the symmetry of the field $G_{\mu\nu}$, the number of freedom degrees is $D(D+1)/2$, also the number of freedom degrees decreases to $(D^2 - D - 2)/2$ due to Eq. (A3). In case of a spin-2 particle, the sum over polarizations $\varepsilon^{\mu\nu}(\mathbf{p}, \lambda)$, takes the form:

$$P^{\mu\nu\alpha\beta} = \sum_\lambda \varepsilon^{\mu\nu}(\mathbf{p}, \lambda) \varepsilon^{\alpha\beta}(\mathbf{p}, \lambda) = \frac{1}{2} (P^{\mu\alpha} P^{\nu\beta} + P^{\mu\beta} P^{\nu\alpha}) - \frac{1}{D-1-\xi} P^{\mu\nu} P^{\alpha\beta}, \quad (\text{A4})$$

and the propagator of the tensor mediator reads as:

$$D_G^{\mu\nu\alpha\beta}(p) = i P^{\mu\nu\alpha\beta} / (p^2 - m_G^2), \quad (\text{A5})$$

where $P^{\mu\nu} = -\eta^{\mu\nu} + (1 - \xi)p^\mu p^\nu / m_G^2$ is the expressions for the sum over polarizations of a vector particle; $\xi = 1$ is Feynman gauge (massless graviton) and $\xi = 0$ is Landau gauge (massive graviton).

Appendix B: Matrix element

The amplitude squared for the process $lN \rightarrow lNG$ reads

$$|\mathcal{A}_{2 \rightarrow 3}^G|^2 = \frac{R^{(0)} + R^{(2)}m_l^2 + R^{(4)}m_l^4}{12m_G^4 \tilde{s}^2 \tilde{u}^2 [\tilde{s} + \tilde{u} + t - m_G^2]^2}, \quad (\text{B1})$$

where the typical terms are expressed through the sums

$$R^{(0)} = \sum_{i=0}^6 m_G^{2*i} R_i^{(0)}, \quad R^{(2)} = \sum_{i=1}^5 m_G^{2*i} R_i^{(2)}, \quad R^{(4)} = \sum_{i=2}^4 m_G^{2*i} R_i^{(4)}, \quad (B2)$$

$$R_6^{(0)} = 3 \{ \tilde{s}^2 [P^2 t - 4(p', P)^2] - 2\tilde{s}\tilde{u} [P^2 t + 4(p, P)(p', P)] + \tilde{u}^2 [P^2 t - 4(p, P)^2] \}, \quad (B3)$$

$$\begin{aligned} R_5^{(0)} = & 3\tilde{s}^3 \{ P^2(\tilde{u} - 2t) + 8(p', P)^2 \} + \\ & + 6\tilde{s}^2 \{ P^2 [-t^2 + 2t\tilde{u} + 4\tilde{u}^2] + 8(p, P)(p', P)\tilde{u} + 4(p', P)^2 [t + \tilde{u}] \} + \\ & + 3\tilde{s}\tilde{u} \{ 14P^2 t^2 + 4P^2 t\tilde{u} + P^2 \tilde{u}^2 \} + \\ & + 3\tilde{s}\tilde{u} \{ -4t [(p, P)^2 - 12(p, P)(p', P) + (p', P)^2] + 8(p, P)\tilde{u} [(p, P) + 2(p', P)] \} + \\ & + 6\tilde{u}^2 \{ t + \tilde{u} \} \{ 4(p, P)^2 - P^2 t \}, \end{aligned} \quad (B4)$$

$$\begin{aligned} R_4^{(0)} = & -3 \{ \tilde{s}^4 [-P^2 t + 2P^2 \tilde{u} + 4(p', P)^2] + \\ & + 2\tilde{s}^3 [P^2 [-t^2 + 3t\tilde{u} + 9\tilde{u}^2] + 4(p, P)(p', P)\tilde{u} + 4(p', P)^2 [t + \tilde{u}]] + \\ & + \tilde{s}^2 [P^2 [-t^3 + 30t^2\tilde{u} + 26t\tilde{u}^2 + 18\tilde{u}^3] + 4(p, P)^2 \tilde{u} [\tilde{u} - 2t]] + \\ & + \tilde{s}^2 [16(p, P)(p', P)\tilde{u} [5t + \tilde{u}] + 4(p', P)^2 [t^2 + \tilde{u}^2]] + \\ & + 2\tilde{s}\tilde{u} [P^2 [15t^3 + 15t^2\tilde{u} + 3t\tilde{u}^2 + \tilde{u}^3] + 4(p, P)^2 [\tilde{u}^2 - 3t^2]] + \\ & + 2\tilde{s}\tilde{u} [4(p, P)(p', P) [t + \tilde{u}] [9t + \tilde{u}] - 4(p', P)^2 t [3t + \tilde{u}]] + \\ & + \tilde{u}^2 [t + \tilde{u}]^2 [4(p, P)^2 - P^2 t] \}, \end{aligned} \quad (B5)$$

$$\begin{aligned} R_3^{(0)} = & \tilde{s}\tilde{u} \{ 3\tilde{s}^4 P^2 + 6\tilde{s}^3 P^2 [2t + 7\tilde{u}] + \\ & + 3\tilde{s}^2 [P^2 [23t^2 + 32t\tilde{u} + 18\tilde{u}^2] - 4(p, P)^2 t + 40(p, P)(p', P)t - 4(p', P)^2 t] - \\ & - 2\tilde{s} [-P^2 [69t^3 + 82t^2\tilde{u} + 48t\tilde{u}^2 + 21\tilde{u}^3] + 24(p, P)^2 t [2t + \tilde{u}]] - \\ & - 2\tilde{s} [-12(p, P)(p', P)t [9t + 8\tilde{u}] + 12(p', P)^2 t [5t + 2\tilde{u}]] + \\ & + 3 [P^2 [t + \tilde{u}] [26t^3 + 20t^2\tilde{u} + 3t\tilde{u}^2 + \tilde{u}^3] - 4(p, P)^2 t [t + \tilde{u}] [9t + \tilde{u}]] + \\ & + 3 [+8(p, P)(p', P)t [t + \tilde{u}] [4t + 5\tilde{u}] - 4(p', P)^2 t [9t^2 + 8t\tilde{u} + \tilde{u}^2]] \}, \end{aligned} \quad (B6)$$

$$\begin{aligned} R_2^{(0)} = & 4\tilde{s}\tilde{u} \{ -3\tilde{s}^4 P^2 \tilde{u} - 3\tilde{s}^3 [P^2 [t^2 + 3t\tilde{u} + \tilde{u}^2] + 2(p, P)(p', P)t] + \\ & + \tilde{s}^2 [-P^2 [3t + \tilde{u}] [4t^2 + 3t\tilde{u} + 3\tilde{u}^2] + 6(p, P)^2 t [t + \tilde{u}]] + \\ & + \tilde{s}^2 [-6(p, P)(p', P)t [2t + \tilde{u}] + 6(p', P)^2 t [2t + \tilde{u}]] + \\ & + \tilde{s} [3t^3 [-5P^2 t + 6(p, P)^2 - 2(p, P)(p', P) + 8(p', P)^2]] + \\ & + \tilde{s} [-4t^2 \tilde{u} [5P^2 t - 3(p, P)^2 + (p, P)(p', P) - 3(p', P)^2]] + \\ & + \tilde{s} [t\tilde{u}^2 [6 [(p, P)^2 - (p, P)(p', P) + (p', P)^2] - 13P^2 t] - 9P^2 t\tilde{u}^3 - 3P^2 \tilde{u}^4] - \\ & - 3t [t + \tilde{u}] [t [2t + \tilde{u}] [P^2 [t + \tilde{u}] - 2(p', P)^2]] - \\ & - 3t [t + \tilde{u}] [-4(p, P)^2 t [t + \tilde{u}] + 2(p, P)(p', P)\tilde{u} [t + \tilde{u}]] \}, \end{aligned} \quad (B7)$$

$$\begin{aligned} R_1^{(0)} = & 2\tilde{s}^2 t^2 \tilde{u}^2 \{ -7\tilde{s}^2 P^2 + 4\tilde{s} [-5P^2 t + 6(p, P)^2 - 6(p, P)(p', P) + 8(p', P)^2] - \\ & - 14\tilde{s} P^2 \tilde{u} + 4\tilde{u} [-5P^2 t + 8(p, P)^2 - 6(p, P)(p', P) + 6(p', P)^2] + \\ & + 4t [-3P^2 t + 7(p, P)^2 - 2(p, P)(p', P) + 7(p', P)^2] - 7P^2 \tilde{u}^2 \}, \end{aligned} \quad (B8)$$

$$\begin{aligned} R_0^{(0)} = & 2\tilde{s}^2 t^2 \tilde{u}^2 \{ -\tilde{s}^3 P^2 - \tilde{s}^2 [P^2 [t + 3\tilde{u}] + 4(p', P) [(p', P) - 2(p, P)]] - \\ & - 2\tilde{s}\tilde{u} [P^2 t + 4 [(p, P)^2 - 3(p, P)(p', P) + (p', P)^2]] - \\ & - 3\tilde{s} P^2 \tilde{u}^2 - 4\tilde{s} t [(p, P) - (p', P)]^2 - \\ & - \tilde{u}^2 [P^2 [t + \tilde{u}] + 4(p, P) [(p, P) - 2(p', P)]] - 4t\tilde{u} [(p, P) - (p', P)]^2 \}. \end{aligned} \quad (B9)$$

$$R_5^{(2)} = 4 \{ \tilde{s}^2 [4(p', P)^2 - P^2 t] + 2\tilde{s}\tilde{u} [5P^2 t + 4(p, P)(p', P)] + \tilde{u}^2 [4(p, P)^2 - P^2 t] \} \quad (\text{B10})$$

$$\begin{aligned} R_4^{(2)} = & \tilde{s}^3 \{ 8P^2 t - 34P^2 \tilde{u} - 32(p', P)^2 \} - \\ & - 4\tilde{s}^2 \{ P^2 [-2t^2 + 42t\tilde{u} - 7\tilde{u}^2] + 16(p, P)(p', P)\tilde{u} + 8(p', P)^2 [t + \tilde{u}] \} + \\ & + 2\tilde{s}\tilde{u} \{ 4t [-22P^2 t + 17(p, P)^2 + 6(p, P)(p', P) + 17(p', P)^2] \} + \\ & + 2\tilde{s}\tilde{u} \{ -4\tilde{u} [21P^2 t + 4(p, P) [(p, P) + 2(p', P)]] - 17P^2 \tilde{u}^2 \} - \\ & - 8\tilde{u}^2 \{ t + \tilde{u} \} \{ 4(p, P)^2 - P^2 t \} \end{aligned} \quad (\text{B11})$$

$$\begin{aligned} R_3^{(2)} = & -4 \{ \tilde{s}^4 [P^2 [t - 11\tilde{u}] - 4(p', P)^2] - \\ & - \tilde{s}^3 [P^2 [-2t^2 + 53t\tilde{u} + 9\tilde{u}^2] + 8(p, P)(p', P)\tilde{u} + 8(p', P)^2 [t - 2\tilde{u}]] + \\ & + \tilde{s}^2 [P^2 [t + \tilde{u}] [t^2 - 99t\tilde{u} - 9\tilde{u}^2] + 4(p, P)^2 \tilde{u} [11t - \tilde{u}]] + \\ & + \tilde{s}^2 [8(p, P)(p', P)\tilde{u} [7t + 4\tilde{u}] - 4(p', P)^2 [t^2 - 25t\tilde{u} + \tilde{u}^2]] + \\ & + \tilde{s}\tilde{u} [-P^2 [58t^3 + 98t^2\tilde{u} + 53t\tilde{u}^2 + 11\tilde{u}^3] + 4(p, P)^2 [17t^2 + 25t\tilde{u} + 4\tilde{u}^2]] + \\ & + \tilde{s}\tilde{u} [8(p, P)(p', P) [6t^2 + 7t\tilde{u} - \tilde{u}^2] + 4(p', P)^2 t [17t + 11\tilde{u}]] - \\ & - \tilde{u}^2 [t + \tilde{u}]^2 [4(p, P)^2 - P^2 t] \} \end{aligned} \quad (\text{B12})$$

$$\begin{aligned} R_2^{(2)} = & 2\tilde{s}\tilde{u} \{ -5\tilde{s}^4 P^2 + 4\tilde{s}^3 [-7P^2 t - 2P^2 \tilde{u} + 12(p', P)^2] + \\ & + \tilde{s}^2 [t [-85P^2 t + 20(p, P)^2 + 72(p, P)(p', P) + 196(p', P)^2] - 84P^2 t\tilde{u}] + \\ & + \tilde{s}^2 [-6P^2 \tilde{u}^2 + 48(p', P)\tilde{u} [2(p, P) + (p', P)]] + \\ & + 2\tilde{s} [8t^2 [-7P^2 t + 6(p, P)^2 + 8(p, P)(p', P) + 14(p', P)^2]] + \\ & + 2\tilde{s} [t\tilde{u} [-85P^2 t + 52(p, P)^2 + 184(p, P)(p', P) + 52(p', P)^2]] + \\ & + 2\tilde{s} [6\tilde{u}^2 [4(p, P) [(p, P) + 2(p', P)] - 7P^2 t] - 4P^2 \tilde{u}^3] + \\ & + 4t^3 [-12P^2 t + 17(p, P)^2 + 14(p, P)(p', P) + 17(p', P)^2] + \\ & + 16t^2 \tilde{u} [-7P^2 t + 14(p, P)^2 + 8(p, P)(p', P) + 6(p', P)^2] + \\ & + t\tilde{u}^2 [-85P^2 t + 196(p, P)^2 + 72(p, P)(p', P) + 20(p', P)^2] + \\ & + 4\tilde{u}^3 [12(p, P)^2 - 7P^2 t] - 5P^2 \tilde{u}^4 \} \end{aligned} \quad (\text{B13})$$

$$\begin{aligned} R_1^{(2)} = & 4\tilde{s}t\tilde{u} \{ -\tilde{s}^4 P^2 + \tilde{s}^3 [-3P^2 t - 4P^2 \tilde{u} + 8(p, P)(p', P)] + \\ & + \tilde{s}^2 [\tilde{u} [8 [(p, P)^2 + (p, P)(p', P) + (p', P)^2] - 9P^2 t]] + \\ & + \tilde{s}^2 [-2t [P^2 t + 2 [(p, P)^2 - 4(p, P)(p', P) + (p', P)^2]] - 6P^2 \tilde{u}^2] + \\ & + \tilde{s} [\tilde{u}^2 [8 [(p, P)^2 + (p, P)(p', P) + (p', P)^2] - 9P^2 t]] + \\ & + \tilde{s} [-4t\tilde{u} [P^2 t + 6(p, P)^2 - 16(p, P)(p', P) + 6(p', P)^2]] + \\ & + \tilde{s} [-4P^2 \tilde{u}^3 - 4t^2 [(p, P) - (p', P)]^2] - \\ & - \tilde{u} [t + \tilde{u}] [2P^2 t\tilde{u} + P^2 \tilde{u}^2 + 4t [(p, P) - (p', P)]^2 - 8(p, P)(p', P)\tilde{u}] \} \end{aligned} \quad (\text{B14})$$

$$R_4^{(4)} = -32 \{ \tilde{s}^2 [P^2 t - 4(p', P)^2] + 2\tilde{s}\tilde{u} [P^2 t - 4(p, P)(p', P)] + \tilde{u}^2 [P^2 t - 4(p, P)^2] \} \quad (\text{B15})$$

$$\begin{aligned} R_3^{(4)} = & 64 [\tilde{s} + t + \tilde{u}] \{ \tilde{s}^2 [P^2 t - 4(p', P)^2] + \\ & + 2\tilde{s}\tilde{u} [P^2 t - 4(p, P)(p', P)] + \tilde{u}^2 [P^2 t - 4(p, P)^2] \} \end{aligned} \quad (\text{B16})$$

$$\begin{aligned} R_2^{(4)} = & -32 [\tilde{s} + t + \tilde{u}]^2 \{ \tilde{s}^2 [P^2 t - 4(p', P)^2] + \\ & + 2\tilde{s}\tilde{u} [P^2 t - 4(p, P)(p', P)] + \tilde{u}^2 [P^2 t - 4(p, P)^2] \} \end{aligned} \quad (\text{B17})$$

- [1] L. Bergstrom, *Annalen Phys.* **524**, 479 (2012), [arXiv:1205.4882 \[astro-ph.HE\]](#).
- [2] G. Bertone and D. Hooper, *Rev. Mod. Phys.* **90**, 045002 (2018), [arXiv:1605.04909 \[astro-ph.CO\]](#).
- [3] M. Cirelli, A. Strumia, and J. Zupan, (2024), [arXiv:2406.01705 \[hep-ph\]](#).
- [4] G. Bertone, D. Hooper, and J. Silk, *Phys. Rept.* **405**, 279 (2005), [arXiv:hep-ph/0404175](#).
- [5] G. B. Gelmini, in *Theoretical Advanced Study Institute in Elementary Particle Physics: Journeys Through the Precision Frontier: Amplitudes for Colliders* (2015) pp. 559–616, [arXiv:1502.01320 \[hep-ph\]](#).
- [6] T. Aoyama *et al.*, *Phys. Rept.* **887**, 1 (2020), [arXiv:2006.04822 \[hep-ph\]](#).
- [7] M. Davis, G. Efstathiou, C. S. Frenk, and S. D. M. White, *Astrophys. J.* **292**, 371 (1985).
- [8] P. A. R. Ade *et al.* (Planck), *Astron. Astrophys.* **594**, A13 (2016), [arXiv:1502.01589 \[astro-ph.CO\]](#).
- [9] N. Aghanim *et al.* (Planck), *Astron. Astrophys.* **641**, A6 (2020), [Erratum: *Astron. Astrophys.* 652, C4 (2021)], [arXiv:1807.06209 \[astro-ph.CO\]](#).
- [10] B. W. Lee and S. Weinberg, *Phys. Rev. Lett.* **39**, 165 (1977).
- [11] E. W. Kolb and K. A. Olive, *Phys. Rev. D* **33**, 1202 (1986).
- [12] G. Krnjaic, *Phys. Rev. D* **94**, 073009 (2016), [arXiv:1512.04119 \[hep-ph\]](#).
- [13] J. McDonald, *Phys. Rev. D* **50**, 3637 (1994), [arXiv:hep-ph/0702143](#).
- [14] C. P. Burgess, M. Pospelov, and T. ter Veldhuis, *Nucl. Phys. B* **619**, 709 (2001), [arXiv:hep-ph/0011335](#).
- [15] J. D. Wells, , 283 (2008), [arXiv:0803.1243 \[hep-ph\]](#).
- [16] R. M. Schabinger and J. D. Wells, *Phys. Rev. D* **72**, 093007 (2005), [arXiv:hep-ph/0509209](#).
- [17] G. Bickendorf and M. Drees, *Eur. Phys. J. C* **82**, 1163 (2022), [arXiv:2206.05038 \[hep-ph\]](#).
- [18] E. E. Boos, V. E. Bunichev, and S. S. Trykov, *Phys. Rev. D* **107**, 075021 (2023), [arXiv:2205.07364 \[hep-ph\]](#).
- [19] H. Sieber, D. V. Kirpichnikov, I. V. Voronchikhin, P. Crivelli, S. N. Gninenko, M. M. Kirsanov, N. V. Krasnikov, L. Molina-Bueno, and S. K. Sekatskii, *Phys. Rev. D* **108**, 056018 (2023), [arXiv:2305.09015 \[hep-ph\]](#).
- [20] R. Catena and T. R. Gray, *JCAP* **11**, 058 (2023), [arXiv:2307.02207 \[hep-ph\]](#).
- [21] B. Holdom, *Phys. Lett. B* **166**, 196 (1986).
- [22] E. Izaguirre, G. Krnjaic, P. Schuster, and N. Toro, *Phys. Rev. Lett.* **115**, 251301 (2015), [arXiv:1505.00011 \[hep-ph\]](#).
- [23] R. Essig, P. Schuster, N. Toro, and B. Wojtsekhowski, *JHEP* **02**, 009 (2011), [arXiv:1001.2557 \[hep-ph\]](#).
- [24] Y. Kahn, G. Krnjaic, J. Thaler, and M. Tups, *Phys. Rev. D* **91**, 055006 (2015), [arXiv:1411.1055 \[hep-ph\]](#).
- [25] B. Batell, R. Essig, and Z. Surujon, *Phys. Rev. Lett.* **113**, 171802 (2014), [arXiv:1406.2698 \[hep-ph\]](#).
- [26] E. Izaguirre, G. Krnjaic, P. Schuster, and N. Toro, *Phys. Rev. D* **88**, 114015 (2013), [arXiv:1307.6554 \[hep-ph\]](#).
- [27] A. Kachanovich, S. Kovalenko, S. Kuleshov, V. E. Lyubovitskij, and A. S. Zhevlakov, *Phys. Rev. D* **105**, 075004 (2022), [arXiv:2111.12522 \[hep-ph\]](#).
- [28] V. E. Lyubovitskij, A. S. Zhevlakov, A. Kachanovich, and S. Kuleshov, *Phys. Rev. D* **107**, 055006 (2023), [arXiv:2210.05555 \[hep-ph\]](#).
- [29] D. Gorbunov and D. Kalashnikov, *Phys. Rev. D* **107**, 015014 (2023), [arXiv:2211.06270 \[hep-ph\]](#).
- [30] J. Claude, M. Dutra, and S. Godfrey, *Phys. Rev. D* **107**, 075006 (2023), [arXiv:2208.09422 \[hep-ph\]](#).
- [31] W. Wang, W.-L. Xu, J. M. Yang, and R. Zhu, *Nucl. Phys. B* **995**, 116348 (2023), [arXiv:2305.12668 \[hep-ph\]](#).
- [32] H. M. Lee, M. Park, and V. Sanz, *Eur. Phys. J. C* **74**, 2715 (2014), [arXiv:1306.4107 \[hep-ph\]](#).
- [33] Y.-J. Kang and H. M. Lee, *Eur. Phys. J. C* **80**, 602 (2020), [arXiv:2001.04868 \[hep-ph\]](#).
- [34] N. Bernal, M. Dutra, Y. Mambrini, K. Olive, M. Peloso, and M. Pierre, *Phys. Rev. D* **97**, 115020 (2018), [arXiv:1803.01866 \[hep-ph\]](#).
- [35] M. G. Folgado, A. Donini, and N. Rius, *JHEP* **04**, 036 (2020), [arXiv:1912.02689 \[hep-ph\]](#).
- [36] Y.-J. Kang and H. M. Lee, *Eur. Phys. J. C* **81**, 868 (2021), [arXiv:2002.12779 \[hep-ph\]](#).
- [37] M. Dutra, *PoS LeptonPhoton2019*, 076 (2019), [arXiv:1911.11844 \[hep-ph\]](#).
- [38] S. Clery, Y. Mambrini, K. A. Olive, A. Shkerin, and S. Verner, *Phys. Rev. D* **105**, 095042 (2022), [arXiv:2203.02004 \[hep-ph\]](#).
- [39] J. A. Gill, D. Sengupta, and A. G. Williams, *Phys. Rev. D* **108**, L051702 (2023), [arXiv:2303.04329 \[hep-ph\]](#).
- [40] W. Wang, L. Wu, J. M. Yang, H. Zhou, and B. Zhu, *JHEP* **12**, 072 (2020), [Erratum: *JHEP* 02, 052 (2021)], [arXiv:1912.09904 \[hep-ph\]](#).
- [41] A. de Giorgi and S. Vogl, *JHEP* **11**, 036 (2021), [arXiv:2105.06794 \[hep-ph\]](#).
- [42] A. de Giorgi and S. Vogl, *JHEP* **04**, 032 (2023), [arXiv:2208.03153 \[hep-ph\]](#).
- [43] K. Jodłowski, *Phys. Rev. D* **108**, 115017 (2023), [arXiv:2305.05710 \[hep-ph\]](#).
- [44] I. V. Voronchikhin and D. V. Kirpichnikov, *Phys. Rev. D* **106**, 115041 (2022), [arXiv:2210.00751 \[hep-ph\]](#).
- [45] S. N. Gninenko, D. V. Kirpichnikov, M. M. Kirsanov, and N. V. Krasnikov, *Phys. Lett. B* **782**, 406 (2018), [arXiv:1712.05706 \[hep-ph\]](#).
- [46] Y.-S. Liu, D. McKeen, and G. A. Miller, *Phys. Rev. D* **95**, 036010 (2017), [arXiv:1609.06781 \[hep-ph\]](#).
- [47] Y.-S. Liu and G. A. Miller, *Phys. Rev. D* **96**, 016004 (2017), [arXiv:1705.01633 \[hep-ph\]](#).
- [48] D. V. Kirpichnikov, H. Sieber, L. M. Bueno, P. Crivelli, and M. M. Kirsanov, *Phys. Rev. D* **104**, 076012 (2021), [arXiv:2107.13297 \[hep-ph\]](#).
- [49] I. V. Voronchikhin and D. V. Kirpichnikov, (2024), [arXiv:2409.12748 \[hep-ph\]](#).
- [50] E. Fermi, *Nuovo Cim.* **2**, 143 (1925), [arXiv:hep-th/0205086](#).
- [51] C. F. von Weizsacker, *Z. Phys.* **88**, 612 (1934).
- [52] E. J. Williams, *Kong. Dan. Vid. Sel. Mat. Fys. Med.* **13N4**, 1 (1935).
- [53] V. M. Budnev, I. F. Ginzburg, G. V. Meledin, and V. G. Serbo, *Phys. Rept.* **15**, 181 (1975).
- [54] J. Blümlein and J. Brunner, *Phys. Lett. B* **731**, 320 (2014), [arXiv:1311.3870 \[hep-ph\]](#).
- [55] S. Foroughi-Abari and A. Ritz, *Phys. Rev. D* **105**, 095045 (2022), [arXiv:2108.05900 \[hep-ph\]](#).
- [56] S. Foroughi-Abari, P. Reimitz, and A. Ritz, (2024), [arXiv:2409.09123 \[hep-ph\]](#).

- [57] D. Gorbunov and E. Kriukova, *JHEP* **01**, 058 (2024), [arXiv:2306.15800 \[hep-ph\]](#).
- [58] L. Harland-Lang, J. Jaeckel, and M. Spannowsky, *Phys. Lett. B* **793**, 281 (2019), [arXiv:1902.04878 \[hep-ph\]](#).
- [59] D. Gorbunov and E. Kriukova, (2024), [arXiv:2409.11386 \[hep-ph\]](#).
- [60] D. Gorbunov and E. Kriukova (2024) [arXiv:2409.11089 \[hep-ph\]](#).
- [61] D. d’Enterria, M. A. Tamlihat, L. Schoeffel, H.-S. Shao, and Y. Tayalati, *Phys. Lett. B* **846**, 138237 (2023), [arXiv:2306.15558 \[hep-ph\]](#).
- [62] H. M. Lee, M. Park, and V. Sanz, (2024), [arXiv:2412.07850 \[hep-ph\]](#).
- [63] M. G. Folgado, A. Donini, and N. Rius, (2019), [10.1007/JHEP01\(2020\)161](#), [arXiv:1907.04340 \[hep-ph\]](#).
- [64] D. Banerjee *et al.* (NA64), *Phys. Rev. D* **97**, 072002 (2018), [arXiv:1710.00971 \[hep-ex\]](#).
- [65] Y. M. Andreev *et al.* (NA64), *Phys. Rev. Lett.* **132**, 211803 (2024), [arXiv:2401.01708 \[hep-ex\]](#).
- [66] J. Mans (LDMX), *EPJ Web Conf.* **142**, 01020 (2017).
- [67] T. Åkesson *et al.* (LDMX), (2018), [arXiv:1808.05219 \[hep-ex\]](#).
- [68] T. Åkesson *et al.*, in *Snowmass 2021* (2022) [arXiv:2203.08192 \[hep-ex\]](#).
- [69] M. D. Schwartz, *Quantum Field Theory and the Standard Model* (Cambridge University Press, 2014).
- [70] S. D. Drell and J. D. Walecka, *Annals Phys.* **28**, 18 (1964).
- [71] V. B. Berestetskii, E. M. Lifshitz, and L. P. Pitaevskii, *QUANTUM ELECTRODYNAMICS*, Course of Theoretical Physics, Vol. 4 (Pergamon Press, Oxford, 1982).
- [72] T. Beranek, H. Merkel, and M. Vanderhaeghen, *Phys. Rev. D* **88**, 015032 (2013), [arXiv:1303.2540 \[hep-ph\]](#).
- [73] C. F. Perdrisat, V. Punjabi, and M. Vanderhaeghen, *Prog. Part. Nucl. Phys.* **59**, 694 (2007), [arXiv:hep-ph/0612014](#).
- [74] J. D. Bjorken, R. Essig, P. Schuster, and N. Toro, *Phys. Rev. D* **80**, 075018 (2009), [arXiv:0906.0580](#).
- [75] Y.-S. Tsai, *Rev. Mod. Phys.* **46**, 815 (1974).
- [76] L. I. Schiff, *Phys. Rev.* **92**, 988 (1953), [Erratum: *Phys. Rev.* **93**, 1434–1434 (1954)].
- [77] K. J. Kim and Y.-S. Tsai, *Phys. Rev. D* **8**, 3109 (1973).
- [78] C.-Y. Chen, M. Pospelov, and Y.-M. Zhong, *Phys. Rev. D* **95**, 115005 (2017), [arXiv:1701.07437 \[hep-ph\]](#).
- [79] Y. Kahn, G. Krnjaic, N. Tran, and A. Whitbeck, *JHEP* **09**, 153 (2018), [arXiv:1804.03144 \[hep-ph\]](#).
- [80] M. Bondi, A. Celentano, R. R. Dusaev, D. V. Kirpichnikov, M. M. Kirsanov, N. V. Krasnikov, L. Marsicano, and D. Shchukin, *Comput. Phys. Commun.* **269**, 108129 (2021), [arXiv:2101.12192 \[hep-ph\]](#).
- [81] B. B. Oberhauser *et al.*, *Comput. Phys. Commun.* **300**, 109199 (2024), [arXiv:2401.12573 \[hep-ph\]](#).
- [82] I. V. Voronchikhin and D. V. Kirpichnikov, *Phys. Rev. D* **107**, 115034 (2023), [arXiv:2304.14052 \[hep-ph\]](#).
- [83] J. D. Bjorken, S. Ecklund, W. R. Nelson, A. Abashian, C. Church, B. Lu, L. W. Mo, T. A. Nunamaker, and P. Rassmann, *Phys. Rev. D* **38**, 3375 (1988).
- [84] Y. M. Andreev *et al.* (NA64), *Phys. Rev. D* **106**, 032015 (2022), [arXiv:2206.03101 \[hep-ex\]](#).
- [85] A. Berlin, N. Blinov, G. Krnjaic, P. Schuster, and N. Toro, *Phys. Rev. D* **99**, 075001 (2019), [arXiv:1807.01730 \[hep-ph\]](#).
- [86] L. Marsicano, M. Battaglieri, M. Bondi, C. D. R. Carvalho, A. Celentano, M. De Napoli, R. De Vita, E. Nardi, M. Raggi, and P. Valente, *Phys. Rev. D* **98**, 015031 (2018), [arXiv:1802.03794 \[hep-ex\]](#).
- [87] S. Andreas, C. Niebuhr, and A. Ringwald, *Phys. Rev. D* **86**, 095019 (2012), [arXiv:1209.6083 \[hep-ph\]](#).
- [88] K. Hinterbichler, *Rev. Mod. Phys.* **84**, 671 (2012), [arXiv:1105.3735 \[hep-th\]](#).
- [89] C. de Rham, *Living Rev. Rel.* **17**, 7 (2014), [arXiv:1401.4173 \[hep-th\]](#).
- [90] M. Fierz and W. Pauli, *Proc. Roy. Soc. Lond. A* **173**, 211 (1939).